Frictional behaviour of non-crimp fabrics (NCFs) in contact with a forming tool

Evangelos I. Avgoulas [a], Daniel M. Mulvihill [b], Andreas Endruweit [c], Michael P.F. Sutcliffe [a,*], Nicholas A. Warrior [c], Davide S.A. De Focatiis [c], Andrew C. Long [c]

[a] Department of Engineering, University of Cambridge, Trumpington Street, Cambridge, CB2 1PZ, United Kingdom
[b] School of Engineering, James Watt South Building, University of Glasgow, Glasgow, G12 8QQ, United Kingdom
[c] Composites Research Group, Faculty of Engineering, University of Nottingham, University Park, Nottingham, NG7 2RD, United Kingdom

ARTICLE INFO

ABSTRACT

Microscopic observation and analysis are used to examine the role that contact conditions play in determining the frictional behaviour of non-crimp fabrics (NCFs). The true fibre contact length is measured over a range of normal pressures. For the NCF considered, the contact length is 67% lower than for a corresponding unidirectional tow-on-tool contact at a pressure of 240 kPa. The difference in contact behaviour is associated with the fabric architecture, specifically stitching and gaps between tows. These microscopic observations are used to predict friction using a constant interface shear strength model. These predictions are found to compare well with macroscopic friction measurements taken using a sliding sled arrangement, once the roughness of the sled tool is taken into account.

1. Introduction

The use of carbon fibre reinforced plastics (CFRP) is growing in the automotive, aerospace and marine industries, meeting the need to produce lightweight and geometrically complex parts and allowing lower stiffness to weight ratios than traditional metal based structures. A variety of forming techniques can be used to produce these parts from either dry fibre preforms or prepregs. Non-crimp fabric (NCF) composites are reinforced with multiple layers of straight (i.e. non-crimped) fibrous yarns stitched together using polyester thread, aramid or glass yarn [1]. Compared to woven fabrics, NCFs could offer better mechanical performance, shorter process cycles with lower resin consumption, and thus reduced manufacturing costs. Therefore, NCFs are increasingly being considered by the aircraft industry, as well as in automotive applications, wind turbine blades, yachts and other complex structural components [2–4].

Where liquid composite moulding (LCM) processes are employed for component manufacture, a dry preforming process typically precedes the resin infusion stage. The optimum setup of this preforming process to avoid wrinkling and buckling is typically determined by an inefficient trial and error approach. An accurate description of the forces induced in the fabric during preforming is needed to inform predictive models and accurately anticipate deformation including defects such as wrinkling and buckling. A key parameter required to determine the forces acting on the system is the friction in the system, for example for fibre-tool and fibre-fibre contact. Lee et al. [5] used a finite element analysis to show that non-isothermal stamping of woven composites is sensitive to the assumed friction law, predicting significant changes in load and local deformations, a result confirmed by Gorczyca et al. [6]. Hence there is a strong need for better models of friction in composites forming. However such models are held back by a lack of understanding of the mechanisms controlling friction. The aim of this paper is to uncover the mechanisms controlling friction in NCFs, and to make the link between microscopic contact conditions and macroscopic friction.

To better comprehend friction forces, it is important to understand the true fibre-tool and fibre-fibre contact area. In contacts between a fibrous material and any other material, the friction behaviour does not follow the direct proportionality between friction force F and normal force W given by Amontons' first law of friction [7]:

$$F = \mu W \tag{1}$$

where μ is the coefficient of friction. Instead, a more general power law formula has been proposed [8]:

---

* Corresponding author.
  E-mail address: mpfs@eng.cam.ac.uk (M.P.F. Sutcliffe).

$$F = kW^n \tag{2}$$

where k and n are constants. This general description (with n usually less than unity) has been experimentally observed for individual fibres [9–11], multi-fibre arrangements [12,13] and carbon fibre tows [14]. To understand the reasons behind this behaviour, it is helpful first to consider contacts between metal surfaces. The work of Bowden and Tabor [15], Archard [16] and Greenwood and Williamson [17] explained why metal surfaces follow the direct proportionality (i.e. $n = 1$) in Amontons' first law: namely, a constant interface shear strength acts over a 'real area of contact' which is only a fraction of the nominal contact area, but which is usually directly proportional to the applied normal load. However, contact involving fibrous materials deviates from the behaviour associated with metals because the real contact area is generally not linearly proportional to normal load owing to the differing details of the fibre contacts.

To explore the details of the contact behaviour for fibrous material, Smerdova and Sutcliffe [18,19] developed an optical technique to measure the true fibre contact length in woven fabric-tool contact. This was extended by Mulvihill et al. [14] to study the contact of fibrous tows. A key finding of these studies was that the real fibre contact length is actually much smaller than the maximum contact length that would be predicted by an idealised packing of parallel touching fibres, and that the contact length is especially small and sensitive to load at low pressures (i.e. less than 50 kPa, which is representative of pre-forming). Moreover there is a continuous increase in real fibre contact length with normal pressure which occurs as a fibrous tow is compacted by a flat surface [14].

Mulvihill et al. [14] also introduced a new rig to measure friction and fibre contact length concurrently at a small scale. Although real contact area varies non-linearly with normal load in the case of fibrous materials, Mulvihill et al. [14] found that tows obey a constant interface model of friction where friction and real contact area are proportional through a constant of proportionality representing the interfacial shear strength of the fibre contacts. Roselman and Tabor [11] investigated the contact of a carbon filament with a range of rough metal surfaces. They noted an increase in friction with decreasing surface roughness. This effect was also observed by Mulvihill and Sutcliffe for tow-on-metal contact [20]. This was explained by noting that smoother surfaces allow greater tow conformance with the surface and hence greater contact area and friction.

The above findings illustrate how friction in fibrous fabrics is governed by the details of the fibre contact. The present paper applies the methods developed by Smerdova and Mulvihill for woven fabrics and individual tows to determine the mechanisms controlling friction in NCF-on-tool contacts. The hypothesis is that the stitching and tow geometry in NCFs will change the details of the true fibre contact and friction. Sliding sled tests are used to measure macro-scale friction for the same materials which have undergone microscopic analysis. This allows the link to be made for the first time for such fabrics between microscopic contact conditions and macroscopic friction tests.

2. Experimental methodology

2.1. NCF-on-tool contact tests

The experimental methodology described by Smerdova and Mulvihill [14,18,19] is briefly summarised in this section. Fabric is compressed by a glass slide in a loading rig while under a microscope, allowing visualization of the true contact area between the fabric and a flat tool surface (Fig. 1). The rig is able to apply normal loads W to the NCF via glass plates and to enable concurrent measurement of the true contact length L of carbon fibres in contact with the plate over the range of these normal loads. A key feature of the rig is use of a special semi-reflective coating on one surface of the upper glass plate [18], which enhances the contrast of the contacting fibres. Roughness measurements of the upper and lower
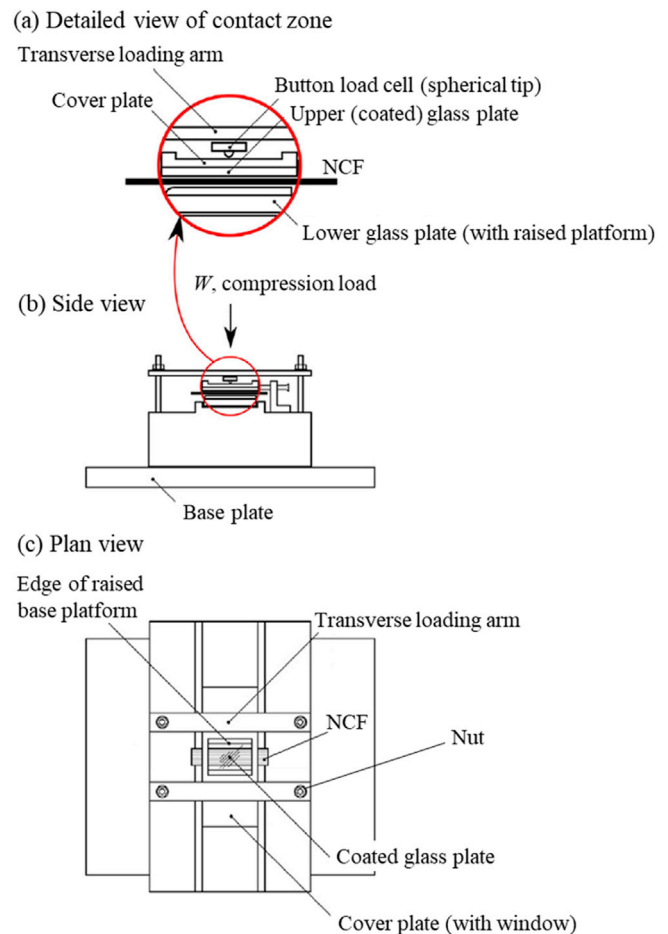

Fig. 1. Schematic drawing of the experimental rig for NCF-on-tool testing. (a) Detailed view of contact zone, (b) side view and (c) plan view, (modified from Ref. [14]).

contact plates were carried out [14] using a stylus profilometer with measured values of R_a of 0.0044 μm and 0.0042 μm, for the upper coated plate and lower platform, respectively.

The biaxial NCF used (FCIM591, supplied by Hexcel, Leicester) is made from 12K carbon tows, weighs 300 g per square metre and contains two tow layers orientated at $-45°/+45°$. The NCF is tricot stitched. This type of NCF was chosen because it is made from the same tow, T700SC-12k-60E, tested by Mulvihill et al. [14], and thus comparison of the contact area results can be made between single tow and NCF measurements. In each test, a layer of the NCF material was cut from the roll and clamped between the lower glass plate and the upper coated glass plate (see Fig. 1). The upper plate was balanced on the top of the NCF fabric with the coating touching the fibres on the triangular tricot stitched side of the NCF. A range of normal loads was applied by tightening the four nuts, with the resulting load measured by two button load cells. Five tests were carried out in total, and each consisted of 14 normal loading steps between 4 N and 200 N. Normal load was taken as the sum of the recorded output of the two button load cells (LBS-25, Interface force measurements, Arizona USA). A new NCF specimen was used for each test as fibre disruption or damage might have occurred during each test. Thus, five separate specimens were tested under the same conditions to give an indication of repeatability. The applied normal load was converted to a nominal pressure p using the nominal contact area of 25 mm × 25 mm.

The load cells were connected through a full bridge amplifier to a desktop PC via a data acquisition device (National Instruments NI USB-6009) and a Lab-VIEW program was written to acquire and output the

load data [14]. A digital camera (Leica DFC295, Leica Microsystems, Switzerland) mounted on an Olympus BX51 M microscope was used to acquire the images using a × 10 objective. This gave a field of view of 1184 μm × 888 μm and a measurement resolution of 0.578 μm. Camera software (Leica Application Suite) was used to scan and stitch together a series of images over a sufficiently large area to produce representative fibre contact length results for the NCF. At each normal load step, a rectangular micro-scale scan area of 7 × 13 images (8.29 mm × 11.54 mm) was imaged covering an area of 1.5 tricot stitching units. In each test, the same portion of the NCF was scanned at each load increment. In these images viewed through the coated glass plate, the fibres appear as distinctive bright strands. An image analysis algorithm [18] implemented using Matlab was used to detect and calculate the fibre contact length. The algorithm uses a filtering process to identify long thin objects (i.e. the fibres in contact with the glass plate). Further details on the algorithm can be found in Mulvihill et al. [14].

Fig. 2a shows the raw micrograph obtained from the microscope and Fig. 2b shows highlighted in red the fibres detected by the algorithm for a typical image (image size: 1184 μm × 888 μm). The total contact length is obtained by adding up the length of individual fibre contacts (as observed in Fig. 2b). Thanks to the semi-reflective coating, the identification of fibres is relatively straightforward with a good quality identification of the contact area in the post-processed image (Fig. 2b) from the raw image (Fig. 2a). Errors in the evaluation of the contact length are assessed in Ref. [18], where differences of up to 20% in the contact length were obtained taking extreme values for relevant parameters. Using more realistic values of the image analysis parameters, the error is expected to be significantly less than 20%. Further details of the methodology and error assessment are given in Ref. [18]. Fig. 2b shows that, for the calculation of contact length, the image analysis process identifies the carbon fibres in contact with the coated glass plate but not the contact with the stitching of the NCF. These stitches are made of a material whose refractive index does not give rise to a bright region at the contact zones, as occurs for the carbon fibre contacts. Although the image resolution is insufficient to evaluate the width of each of the fibre contacts, the total length L of fibres in contact can be accurately determined. Subsequently, the contact area can be estimated (for the circular cross-section fibres used in this study) using a Hertzian contact analysis [14].

2.2. NCF-on-tool macro-scale friction tests

Static and sliding friction forces between the NCF and a horizontal aluminium surface were determined in sled tests (as described in ASTM D 1894, ISO 8295). The roughness of the aluminium surface is characterized by $R_a = 0.5$ μm. The dimensions of the contact interface between sled and aluminium table were 100 mm × 50 mm. A layer of the NCF was attached to a sled. The material roll direction was orientated either parallel or perpendicular to the direction of sled movement and the same side of the fabric was in contact with the tool as per the contact area tests. Vertical forces (normal to the interface between the sled and table) of 10.2, 20.1 and 30.0 N were applied by loading the sled with a weight. The tangential (i.e. horizontal) force exerted on the sled in order to move

it at a constant velocity of 1.67 mm/s was measured using the load cell of an Instron universal testing machine via a light wire through a low friction pulley system. The peak force at the beginning of the test corresponds to the static friction measurement, while the steady-state force corresponds to sliding friction.

3. Results and discussion

3.1. NCF-on-tool true contact length

Fig. 3a shows a representative micrograph of the fibres in contact over the entire scanned area for the highest load level, which corresponds to a nominal normal pressure of 320 kPa. Fig. 3b, c and 3d show the post-processed images of a typical scanned area of 3 × 2 images (3.55 mm × 1.78 mm) for nominal normal pressures of 6.4 kPa (lowest load level), 89.6 kPa and 320 kPa, respectively.

From Fig. 3b–d it can be seen that the microscopic contact behaviour of the NCF fabric tested here has a similar behaviour as that observed for the tow contacts [14], specifically only a small fraction of the fibres make contact with the tool (the areas in red in Fig. 3b–d), with that fraction increasing dramatically with contact pressure.

To quantify the contact length, consider an idealised case with the maximum possible fibre contact length L_{max} corresponding to the situation where all fibres contacting the tool are parallel and touching each other. The normalised fibre contact length is taken as the ratio of the measured fibre contact length L to this ideal maximum length L_{max}. Fig. 4 shows the normalised fibre contact length L/L_{max} (expressed as a percentage) as a function of normal pressure p for the five tests carried out. The average normalised contact length varied from $1.5 \pm 0.3\%$ at 6.4 kPa to $11 \pm 0.77\%$ at 320 kPa.

Tow-on-tool tests showed a normalised fibre contact length of 29.5% at a nominal pressure of 240 kPa [14], while for the NCF-on-tool tests that are described in this paper the normalised fibre contact length is only 9.7% at the same nominal pressure. Thus, although the qualitative picture of the contact conditions for these fabrics is similar to that for the unidirectional tow, quantitatively there is a significant reduction of 67% in the normalised fibre contact length.

Fig. 5 illustrates the reason for this difference in contact behaviour between NCFs and tow contact. Fig. 5a shows a representative micrograph of the entire scanned area at a nominal normal pressure of 320 kPa, while Fig. 5b is an annotated subsection of Fig. 5a. Fig. 5b shows the influence of two factors, stitching and gaps between the tows, affecting the true contact regions identified in red. In the regions around the stitching, highlighted in green in Fig. 5b, the fibres in the carbon tows lose contact with the tool as they lie below the contacting stitching threads. Gaps between the tows (white hatched regions between tows outlined in black in Fig. 5b) also reduce the true fibre contact length by creating areas with minimal fibre contact. These tow gaps was also observed and quantified for woven fabric-on-tool (glass) contact tests [19]. The delineation of the stitching area and tow gaps in Fig. 5b is done manually to understand and inform the results. The separation of the contact area in this way is not used in the quantitative contact area
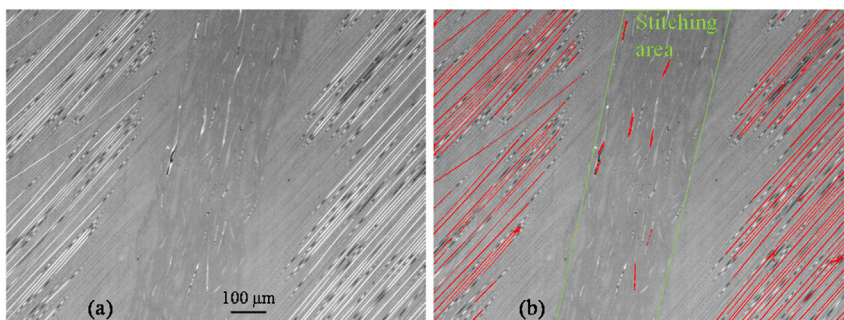

Fig. 2. (A) Raw image from the microscope and (b) post-processed image using the Matlab algorithm which detects the fibres in contact with the coated glass plate (in red). (For interpretation of the references to colour in this figure legend, the reader is referred to the Web version of this article.)
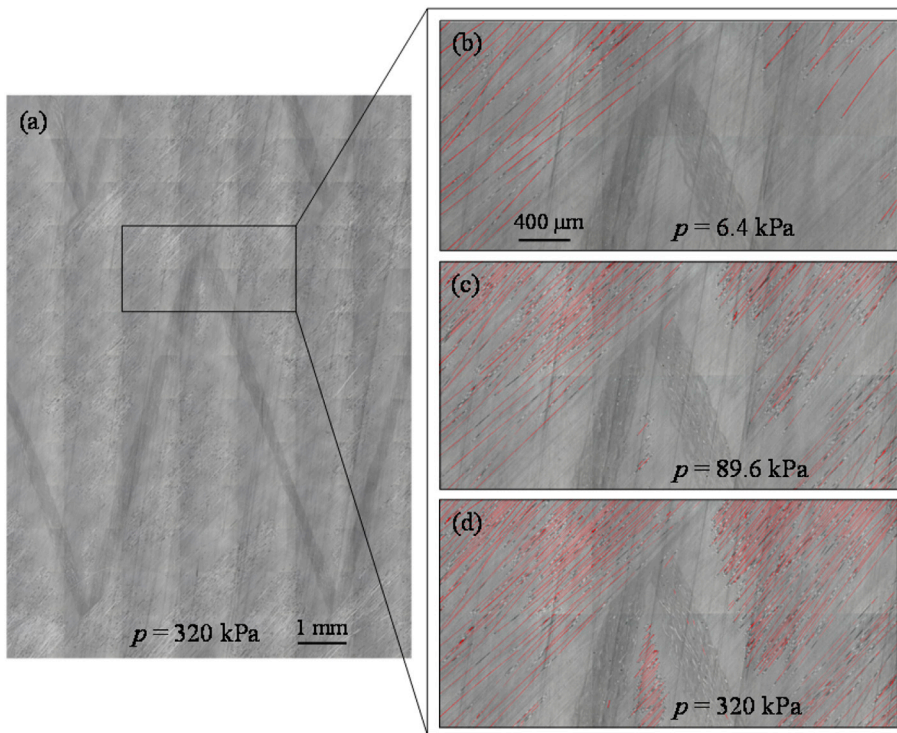
Fig. 3. (A) Raw image from the microscope of the total scanned area for a nominal normal pressure of $p = 320$ kPa. (b), (c) and (d): Part of the post-processed image which detects the fibres in contact with the coated glass plate (in red) for various nominal normal pressures. Results are from one of the five tests. (For interpretation of the references to colour in this figure legend, the reader is referred to the Web version of this article.)
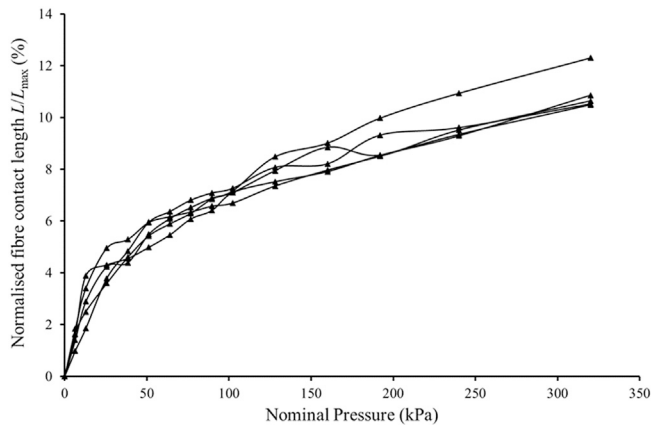

Fig. 4. Effect of nominal pressure p on true fibre contact length L for NCF-on-tool contact, normalised by the idealised contact length L_{max} for parallel touching fibres.
Lines are a guide to the eye.

analysis. These results demonstrate how knowledge about the fabric architecture can lead to a better understanding of the factors influencing the true contact area and hence friction.

3.2. NCF-on-tool true contact area and macro-friction tests

This section aims to make the link between the microscopic measurements of contact area and the macro-friction tests. First the true contact area is inferred from the measured contact length, then a constant shear stress model of friction is used to predict friction from the microscale observations.

The pixel size of the microscope images is 0.578 μm, significantly larger than the average contact width predicted by Hertz theory for the 7 μm diameter fibres (see the analysis below). Hence there is insufficient resolution in the image to measure the width of the contact between the

fibres and the glass plate (tool) accurately. This means that the true fibre contact area cannot be directly measured. However, knowing the filament properties and the true fibre contact length L, an estimation of the true fibre contact area can be made based on a Hertzian contact analysis. According to the Hertzian analysis, the contact half-width a of a cylinder (the fibre) on a flat plane (the glass tool) is given by:

$$a = \sqrt{\frac{2Wd}{\pi E'L}} \qquad (3)$$

where W is the total normal load on the contact patch, d is the fibre diameter (equal to 7 μm), E' is the effective elastic modulus and L is the total true fibre contact length. The effective elastic modulus is given as follows:

$$\frac{1}{E'} = \frac{1 - \nu_{glass}^2}{E_{glass}} + \frac{1 - \nu_{CF}^2}{E_{CF}} \qquad (4)$$

where E_{glass} and E_{CF} are the Young's moduli of the glass plate (tool) and carbon fibre, respectively. The quantities ν_{glass} and ν_{CF} are the Poisson's ratios of the glass plate (tool) and carbon fibre, respectively. The values used for these properties are summarised in Table 1 [21,22]. Because of the nature of the loading condition, the transverse properties were taken for the carbon fibres.

Finally, the true contact area A is given by:

$$A_{entire} = 2aL \qquad (5)$$

Fig. 6 shows the variation with normal load of true fibre contact area A_{entire} obtained from the measured contact lengths via eq. (5) for each of the five tests. A best fit power-law curve is used to draw a smooth line through the average of the five tests. Because the differences in the measured area for the five separate curves are rather small, these curves (identified with black triangles) are superimposed on each other and the mean value given by the orange circle markers. Error bars (e.g. plotting the standard deviation in the results) would be comparable with the size of the circle marker used. The contact area A_{entire} is inferred for the entire NCF contact patch over which the load W was applied (25 mm × 25 mm)
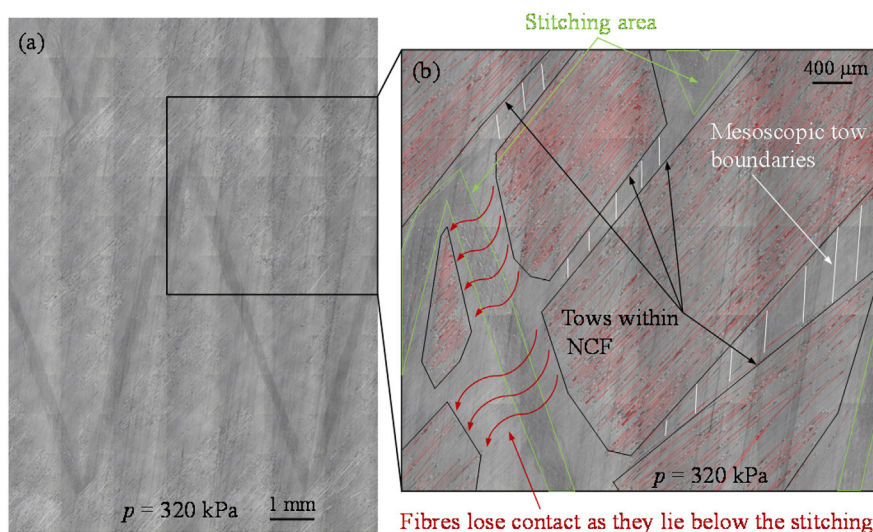
Fig. 5. (A) Raw image from the microscope of the total scanned area. (b) Part of the post-processed image which detects the fibres in contact with the coated glass plate (in red). Fibres lose contact with the tool as they pass below the stitching filaments (in green). Contacting tows within NCF are identified and outlined by hand as black polygons. White lines define gap regions between tows where almost no fibre contact was observed. Nominal normal pressure $p = 320$ kPa. (For interpretation of the references to colour in this figure legend, the reader is referred to the Web version of this article.)

Table 1
Properties of the carbon fibre and the glass plate.

Property	Carbon fibre [21] (transverse direction)	Glass plate [22]
Elastic modulus, E (GPa)	16.5	69
Poisson's ratio, v	0.31	0.24

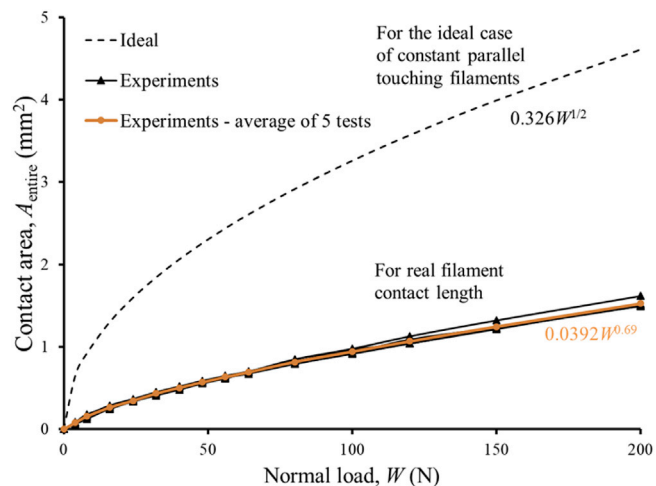**Fig. 6.** True fibre contact area (A_{entire}) against normal load for a 25 mm × 25 mm NCF area. Contact area is calculated from the true fibre contact length using Hertzian contact analysis.

by scaling the contact measurements from the smaller imaged area (8.29 mm × 11.54 mm). For the average contact area results, a power-law fit to the data was found with an exponent n equal to 0.69 and a factor k equal to 0.0392. Fig. 6 includes the theoretical variation of contact area with normal load for the ideal case of parallel touching filaments. In this case, the contact length L is constant for the various loading steps and thus the contact area is proportional to $W^{1/2}$, and k is equal to 0.326.

Having determined the contact conditions between the fabric and the tool, the next step of the analysis is to compare the macro-scale friction results with predictions based on the microscopic contact area calculations.

The measured contact area results presented above can be used to infer a friction response, assuming the constant interface strength model of friction found appropriate for the tows used in the NCF [14]. The curve-fit to the average of the experimental contact area data shown in Fig. 6 is converted to an average shear stress versus average normal pressure prediction in the following way. The theoretical average shear stress τ is taken by multiplying the true contact area A_{entire} by an assumed interface shear strength τ_s, and dividing by the nominal area of contact (i.e. 25 mm × 25 mm). The value of shear stress $\tau_s = 16$ MPa used is taken from Ref. [14], for contact of the same tows as used in the NCF fabric. Similarly the average normal pressure p is given by dividing the normal load W by the nominal area of contact.

Fig. 7 Compares the measured macro-friction results from the sled tests with the predictions from the microscale model. The error bars in Fig. 7 show the sample standard deviation for the five microscopic tests carried out. Note that the first data point from the measured macro-scale contact behaviour corresponds to a normal pressure of 6.4 MPa, so that the normal pressures corresponding to available data for the predicted and measured responses do not overlap. Nevertheless the smooth behaviour for each of these curves supports the validity of the comparison.

An alternative representation of the data, plotting the friction coefficient as a function of normal pressure, is shown in Fig. 8. Note that the pressure scale is logarithmic. The measured friction coefficients are comparable with values for other carbon fabrics; for example Cornelissen et al. [23] find a friction coefficient of around 0.2 for a woven carbon fabric in contact with a reasonably smooth steel foil.

The comparison between the theoretical predictions and the measurements shown in Figs. 7 and 8 is encouraging, especially given the difference in conditions between the microscale measurements and the macro-friction tests. Specifically the macro-scale results are for a relatively rough tool, while the predictions are based on contact with a smooth glass surface. The effect of roughness is to reduce the contact area and friction significantly, with reductions in friction coefficient of around 50% found by Mulvihill at al [20] for roughness amplitudes comparable with those of the sled tests. This effect explains the reduction of friction coefficient of between 25 and 47% for the sled tests compared with predictions from microscale observations, at a pressure of around 6 kPa. Hence these results confirm that the contact behaviour observed for fibre contacts, in conjunction with a constant interface strength model of friction, is a reasonable way to model friction behaviour of these NCF fabrics.

It should be noted that the situation is complicated by the presence of friction at the stitch contacts, which has not been taken into account and
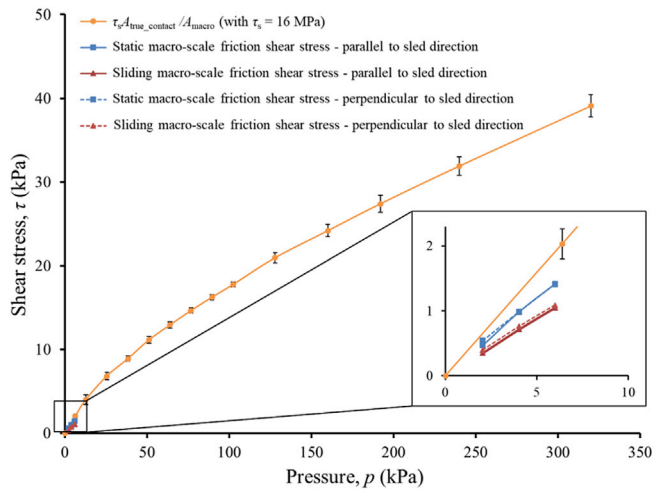
Fig. 7. The effect of normal pressure on the frictional shear stress, comparing macro-scale sled measurements with predictions using the measured fibre contact behaviour (Fig. 6) in conjunction with a constant interfacial shear strength τ_s.
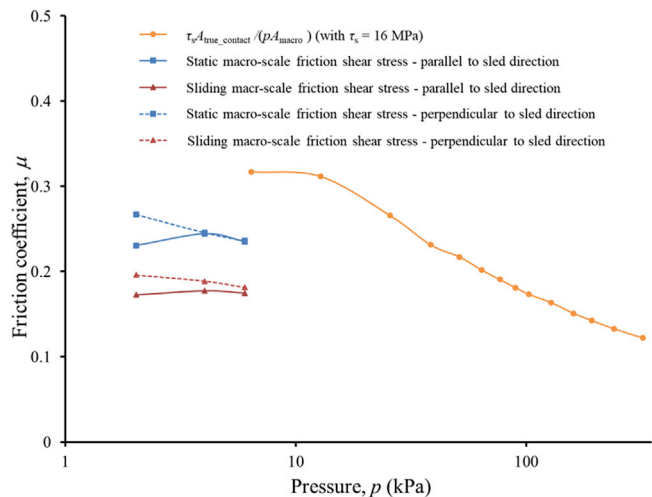

Fig. 8. The effect of normal pressure on the friction coefficient, comparing macro-scale sled measurements with predictions using the measured fibre contact behaviour (Fig. 6) in conjunction with a constant interfacial shear strength τ_s. Note the logarithmic scale for pressure.

which would serve to increase the theoretical predictions of friction. Noting that the area of the stitching is relatively small compared with the carbon tow area (see Fig. 5), it seems likely that the stitching's contribution to friction is also relatively small, making the assumption that the contact area ratio and shear strength in the stitched regions is comparable with that in the tow regions.

As well as the fabric material and architecture, other factors that will affect friction include the presence of binder, tool material and, as mentioned previously, the amplitude of the tool roughness. The importance of these various effects highlights the need to have a sound physics-based understanding of the causes of friction, to allow better characterisation and modelling of the phenomena. For example Mulvihill et al. [20] were able to use an understanding of the interaction between fibres and tool roughness to explain the reduction in observed friction with increasing tool roughness in terms of the reduction in true contact area.

Although it is not expected that the fibre contact measurements described in this paper would be a routine test, understanding the science behind the contact behaviour (for example the interplay between the

stitching, tow flexibility and sizing) can help inform development and interpretation of macroscopic experiments or meso-scale models. In order to extend the results to the wide range of NCFs available, it is expected that the effect of stitching on contact pressure distribution can be reasonable well modelled using existing finite element modelling techniques. The more difficult aspect of friction modelling for NCFs, which this paper addresses, provides understanding of how the contact at this meso-scale translates into true contact area and friction.

4. Conclusions

An experimental investigation has been carried out to measure NCF-on-tool true fibre contact length over a range of normal loads. The average microscopic contact length, expressed as a percentage of the idealised contact length, varied from 1.5% at 6.4 kPa to 11% at 320 kPa. Compared to tow-on-tool tests [14], NCF-on-tool tests showed a 67% reduction of true fibre contact length on the tool surface for a 240 kPa normal pressure. This significant difference can be attributed to the presence of stitching and mesoscopic tow boundaries in NCF which reduce substantially the true contact length of the fibres within the fabric.

Macro-friction tests were carried out using a sled arrangement. The measured true contact length behaviour was used to predict the friction response assuming a constant interface strength model, taking a literature value of interface shear strength of 16 MPa measured for the tows used in the NCF fabric. Hertzian theory was used to predict the width of the fibre contact patches. The predicted frictional behaviour is in reasonable agreement with the measured behaviour, once the effect of tool roughness is taken into account, confirming the validity of the constant interfacial strength model in conjunction with an accurate representation of the true fibre contact area. Hence the work makes a link for the first time between microscopic observations of contact in fibrous fabrics and macroscale friction measurements.

Appendix A. Supplementary data

Supplementary data related to this article can be found at https://doi.org/10.1016/j.triboint.2018.01.026.

References

[1] Kong H, Mouritz AP, Paton R. Tensile extension properties and deformation mechanisms of multiaxial non-crimp fabrics. Compos Struct 2004;66:249–59.
[2] Modular Joints for Aircraft Components (MOJO). Research Project funded by the European Commission within the frame of 6th framework-aeronautics and space. 2006.
[3] Horsting K. Advanced properties of warp knitted multiaxial layer fabric for a rationalized composite production. In: 41st International SAMPE Symposium; March 1996. p. 188–95.
[4] Lomov SV. Non-crimp fabric composites: manufacturing, properties and applications. Woodhead Publishing Limited; 2011. p. 441–95.
[5] Lee W, Um M-K, Byun J-H, Boisse P, Cao J. Numerical study on thermo-stamping of woven fabric composites based on double-dome stretch forming. Int J Material Form 2010;3:S1217–27.
[6] Gorczyca JL, Fetfatsidis KA, Sherwood JA. Friction properties of reinforcements in composites. In: Boisse P, editor. Composites reinforcements for optimum performance. Woodhead Publishing Limited; 2011. p. 397–430.
[7] Amontons G. De la resistance causée dans les machines, Mémoires de l'Académie Royale A;1699:257–282.
[8] Howell HG, Mazur J. Amontons' law and fibre friction. J Text Inst Trans 1953;44(2):59–69.
[9] Howell HG. Inter-fibre friction. J Text Inst Trans 1951;42(12):521–33.
[10] Tabor D. Friction, lubrication and wear of synthetic fibres. Wear 1957;1(1):5–24.

[11] Roselman IC, Tabor D. The friction and wear of individual carbon fibres. J Phys Appl Phys 1977;10(8):1181–94.

[12] Morrow JA. Frictional properties of cotton fibres. J Text Inst Trans 1931;22:425–40.

[13] Bandyopadhyay SB. Frictional properties of jute and some other long vegetable fibers, Part I: general study of characters. Textil Res J 1951;21:659–70.

[14] Mulvihill DM, Smerdova O, Sutcliffe MPF. Friction of carbon fibre tows. Compos Appl Sci Manuf 2017;93:185–98.

[15] Bowden FP, Tabor D. The friction and lubrication of solids. Oxford: Clarendon Press; 1950.

[16] Archard JF. Elastic deformation and the laws of friction. Proc Roy Soc Lond Math Phys Sci 1957;243(1233):190–205.

[17] Greenwood JA, Williamson JBP. Contact of nominally flat surfaces. Proc Roy Soc Lond J. Math. Phys. Eng. Sci. 1966;295(1442):300–19.

[18] Smerdova O, Sutcliffe MPF. Novel experimental method for microscale contact analysis in composite fabric forming. Exp Mech 2015;55(8):1475–83.

[19] Smerdova O, Sutcliffe MPF. Multiscale tool–fabric contact observation and analysis for composite fabric forming. Compos Appl Sci Manuf 2015;73:116–24.

[20] Mulvihill DM, Sutcliffe MPF. Effect of tool surface topography on friction with carbon fibre tows for composite fabric forming. Compos Appl Sci Manuf 2017;93: 199–206.

[21] Mounier D, Poilâne C, Bûcher C, Picart P. Evaluation of transverse elastic properties of fibers used in composite materials by laser resonant ultrasound spectroscopy. Nantes, France: Société Française d'Acoustique; April 2012. Acoustics 2012.

[22] Edupack CES. Cambridge UK: Granta Design Ltd; 2014.

[23] Cornelissen B, Sachs U, Rietman B, Akkerman R. Dry friction characterisation of carbon fibre tow and satin weave fabric for composite applications. Compos Appl Sci Manuf 2014;56:127–35.